

Nanoscale

Accepted Manuscript

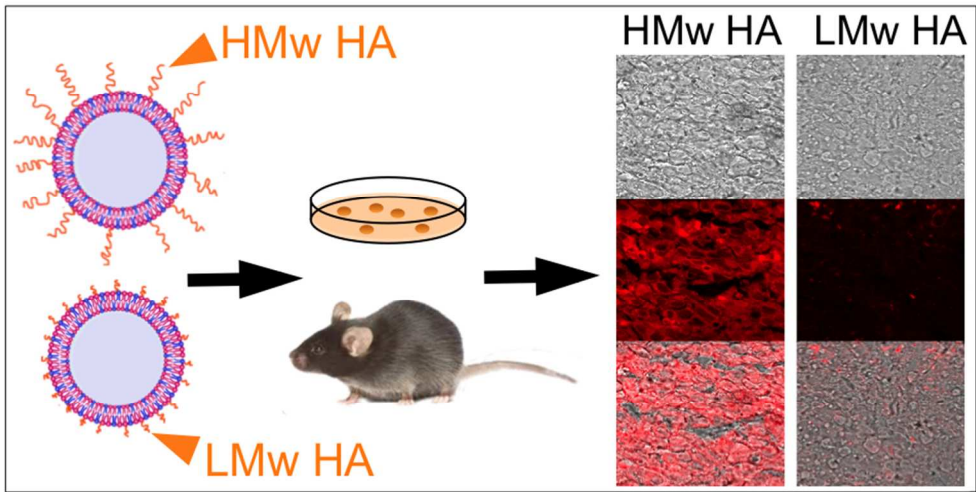


This is an *Accepted Manuscript*, which has been through the Royal Society of Chemistry peer review process and has been accepted for publication.

Accepted Manuscripts are published online shortly after acceptance, before technical editing, formatting and proof reading. Using this free service, authors can make their results available to the community, in citable form, before we publish the edited article. We will replace this *Accepted Manuscript* with the edited and formatted *Advance Article* as soon as it is available.

You can find more information about *Accepted Manuscripts* in the [Information for Authors](#).

Please note that technical editing may introduce minor changes to the text and/or graphics, which may alter content. The journal's standard [Terms & Conditions](#) and the [Ethical guidelines](#) still apply. In no event shall the Royal Society of Chemistry be held responsible for any errors or omissions in this *Accepted Manuscript* or any consequences arising from the use of any information it contains.



82x42mm (300 x 300 DPI)

Cite this: DOI: 10.1039/c0xx00000x

www.rsc.org/xxxxxx

PAPER

Tumor targeting profiling of hyaluronan-coated lipid based-nanoparticles

Shoshy Mizrahy^{a,b,c}, Meir Goldsmith^{a,b,c}, Shani Leviatan-Ben-Arye^{a,b,c}, Einat Kisin-Finfer^d, Orit Redy^d, Srimeenakshi Srinivasan^e, Doron Shabat^d, Biana Godin^e, and Dan Peer^{a,b,c*}

Received (in XXX, XXX) Xth XXXXXXXXX 20XX, Accepted Xth XXXXXXXXX 20XX

DOI: 10.1039/b000000x

Hyaluronan (HA), a naturally occurring high Mw (HMw) glycosaminoglycan, has been shown to have crucial roles in cell growth, embryonic development, healing processes, inflammation, and tumor development and progression. Low Mw (LMw, <10KDa) HA has been reported to provoke inflammatory responses, such as induction of cytokines, chemokines, reactive nitrogen species and growth factors. Herein, we prepared and characterized two types of HA-coated (LMw and HMw) lipid-based targeted and stabilized Nanoparticles (tsNPs) and tested their binding to tumor cells expressing HA receptor (CD44), systemic immunotoxicity, and biodistribution in tumor bearing mice. *In vitro*, the Mw of the surface anchored HA had a significant influence on the affinity towards CD44 on B16F10 murine melanoma cells. LMw HA-tsNPs exhibited weak binding, while binding of tsNPs coated with HMw HA was characterized with high binding. Both types of tsNPs had no measured effect on cytokine induction *in vivo* following intravenous administration to healthy C57BL/6 mice suggesting no immune activation. HMw HA-tsNPs showed enhance circulation time and tumor-targeting specificity, mainly by accumulating in the tumor and its vicinity compared with LMw HA-tsNPs. Finally, we show that entrapping Methotrexate (MTX), a commonly used chemotherapy, in HMw HA-tsNPs slowly diffused from the particles with a half-life of 13.75 days, and improve the therapeutic outcome in a murine B16F10 melanoma model compared with NPs suggesting an active cellular targeting beyond the Enhanced Permeability and Retention (EPR) effect. Taken together, these findings have major implications for the use of high molecular weight HA in nanomedicine as selective and safe active cellular targeting moiety.

1. Introduction

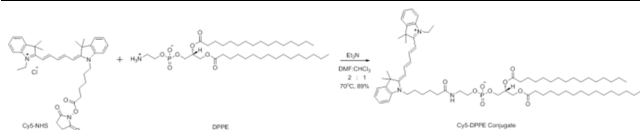
The Hyaluronan (HA) is a naturally occurring linear glycosaminoglycan (GAG) composing parts of the extra cellular matrix (ECM). HA is comprised of alternating disaccharide units³⁰ of d-glucuronic acid and N-acetyl-d-glucosamine with β -(1-4) interglycosidic linkage¹. HA was first considered to play mainly a structural role due to the outstanding hydrodynamic properties especially related to its viscosity and ability to retain water². However, over the years many additional roles of HA³⁵ have been revealed such as its crucial involvement in cell growth, embryonic development, healing processes, inflammation, and tumor development^{2,3}.

As with other components of the ECM, low Mw (LMw) fragments of HA were reported to act as mediators of⁴⁰ inflammation⁴. This is opposed to the non-immunogenic and anti-angiogenic characteristics of high Mw (HMw) HA⁵. The different biological effects reported for HMw and LMw HA have been suggested to be mediated by the HA cell surface receptor CD44. We and others have demonstrated that there is a direct⁴⁵

correlation between HA Mw and its affinity towards CD44⁶⁻⁸. The high affinity of HMw HA (opposed to low affinity for LMw HA) is probably a result of a multivalent binding as HMw HA contains thousands of binding sites. Additional factors also regulate HA-CD44 interaction among which are surface density⁵⁰ of CD44, its many splice variants and most likely different conformation⁹.

However, there is inconsistency in the literature regarding the dependency of HA Mw on the biological functions with respect to inflammation and tumor progression as administration of LMw⁵⁵ HA to tumor xenografts inhibits rather than stimulates tumor growth and overexpression of hyaluronidase suppresses colon and breast carcinoma growth in human xenografts². In addition, reports regarding induction of inflammatory cytokines as a result of LMw HA administration are also inconsistent¹⁰. Several⁶⁰ factors may contribute to these⁵ inconsistent reports, including non-HA contamination (for HA samples of animal or bacterial origin) and the fact that all evidences of the biological effects of LMw HA fragments were based on exogenous addition of HA fragments.⁶⁵

There are several advantages for HMw HA, which make it



Scheme 1: Chemical synthesis of Cy5-DPPE Conjugate

suitable for the use in drug delivery systems (DDS): solubility in water, biodegradability, biocompatibility, lack of toxicity and immunogenicity, and the ease of chemical modification³. As a coating agent for DDS, HMw HA promotes long-term circulation and increased stability that can be attributed to reduction in protein adsorption (corona) and opsonisation¹¹. This feature was successfully adopted from the HA capsule of group A streptococci enables it to escape the host immune response¹². In addition, as the major ligand for CD44 and CD168 (also known as Receptor for Hyaluronan Mediated Motility, RHAMM), HA is suitable for targeting CD44 and RHAMM-expressing cells³. Since both CD44 and CD168 are overexpressed on various tumors, for example, squamous cell carcinoma, ovarian, colon, stomach, glioma, and many types of leukemia, lymphoma and multiple myeloma, the use of HA as a targeting agent is even more attractive¹¹. We and others have demonstrated that HA can be covalently attached to the surface of nanoparticles (NPs) and efficiently target epithelial cancer cells and leukocytes expressing HA receptors^{3, 13-18}. Our previous report focused on the design and characterization of a small library of lipid-based nanoparticles distinguished by the length of their surface-anchored HA, ranging from 6.4 kDa to 1500 kDa⁷. We have shown that the affinity of the targeted and stabilized nanoparticles (tsNPs) towards the CD44 receptor was found to be solely controlled by the Mw of the tsNPs surface-bound HA, from extremely low binding for LMw-HA to binding with high affinity for HMw-HA by Surface Plasmon Resonance (SPR) analysis.

In this study, we focused on two tsNPs having various Mw of anchored HA on their surface LMw HA (<10kDa) and tsNPs HMw HA (>700kDa). The effects of HA Mw on cell binding, immune response, circulation time and tumor localization as well as therapeutic response with MTX as a model drug entrapped in the NPs are investigated and discussed.

2. Experimental

2.1 Materials

Pure Soybean phosphatidylcholine (Phospholipon 90G) was a kind gift from Phospholipid GMBH (Germany). 1,2-dipalmitoyl-sn-glycero-3-phosphoethanolamine (DPPE) and Cholesterol (Chol) were purchased from Avanti Polar Lipids Inc. (Alabaster, AL, USA). Sodium hyaluronate with average Mw of 6.4 kDa and 700 kDa were purchased from Lifecore Biomedical, LLC (MN, USA). Methotrexate (MTX), Ethyl-dimethyl-aminopropyl-carbodiimide (EDC), LPS, paraformaldehyde (PFA) and trypan blue were purchased from Sigma-Aldrich Co. (St. Louis, MO, USA). Sulfo-NHS was purchased from Proteochem. Concavalin A- labeled Alexa 488 (ConA 488) was purchased from Life technologies. 2-(4-Morpholino)ethane Sulfonic Acid (MES) was purchased from Fisher Scientific. Alexa Fluor 488 Rat anti-

human CD44 (Clone # IM7) and IgG2b isotype control antibodies were purchased from BioLegend (San Diego, USA). Milliplex® MAP kit 25-plex Mouse cytokine/chemokine Magnetic bead panel (MCYTOMAG-70K-PMX) was purchased from Millipore. Materials for cell cultures, HEPES and EZ-PCR Mycoplasma Test Kit were purchased from Biological Industries Co. (Beit Haemek, Israel). Tissue-Tek OCT was purchased from Sakura. Florescent mounting medium was purchased from Golden Bridge international, Mukilteo, WA, USA. All other reagents were of analytical grade.

2.2 Methods

2.2.1 Cy5-DPPE Conjugate Synthesis

Cy5-NHS was synthesized according to previously published procedure¹⁹.

Cy5-NHS (27 mg, 0.043 mmol) was dissolved in 2 ml of DMF and 1 ml of CHCl₃. Then 1,2-dipalmitoyl-sn-glycero-3-phosphoethanolamine (DPPE) (30 mg, 0.043 mmol) was added followed by the addition of Et₃N (5.9 μL, 0.043 mmol). The reaction mixture was heated to 70°C and stirred overnight. The reaction was monitored by RP-HPLC (gradient 10-90% ACN in H₂O, 20 min). Upon completion, the solvent was removed under reduced pressure and the crude product was purified by column chromatography on silica gel (3:7 MeOH: DCM) to afford Cy5-DPPE conjugate (45 mg, 89%) as a blue solid. (See Scheme 1).

¹H NMR (400 MHz, CDCl₃): δ = 8.35 (1H, brs), 7.86 (2H, quart, J = 8.8 Hz), 7.39-7.32 (4H, m), 7.24-7.15 (4H, m), 7.09 (1H, d, J = 7.8 Hz), 6.94 (1H, t, J = 9.5 Hz), 6.52 (1H, d, J = 13.3 Hz), 6.40 (1H, d, J = 13.3 Hz), 5.22 (1H, m), 4.41 (1H, dd, J = 11.8, 3 Hz), 4.19-4.10 (5H, m), 4.05-4.02 (4H, m), 3.48 (2H, m), 2.32-2.22 (6H, m), 1.85 (2H, m), 1.77-1.72 (2H, m), 1.70 (6H, s), 1.69 (6H, s), 1.55-1.53 (4H, m), 1.40-1.36 (2H, m), 1.23 (48H, m), 0.87 (9H, m). MS (ES-): m/z calc. for C₇₀H₁₁₂N₃O₉P: 1169.8; found: 1171.1 (M+H)⁺. HPLC grad. 10-90% ACN in water 20 min, retention time- 14.5 min, λ = 640 nm.

2.2.2 Preparation of lipid NPs and encapsulation of MTX

Multilamellar vesicles (MLV) composed of PC:Chol:DPPE at mole ratios of 60:20:20, were prepared by the traditional lipid-film method^{16, 17, 20, 21}. MLVs prepared for confocal analysis contained 0.1% Cy5 labeled DPPE. Briefly, the lipids were dissolved in ethanol, evaporated to dryness under reduced pressure in a rotary evaporator (Buchi Rotary Evaporator Vacuum System Flawil, Switzerland) and hydrated by the PBS swelling solution at pH 7.4 or with MTX (1.5mg/mL) in PBS solution at pH 7.4. This was followed by extensive agitation using a vortex device and a 2 h incubation in a shaker bath at 37 °C. The MLV were extruded through a Lipex extrusion device (Nortnen lipids, Vancouver, Canada), operated at 65 °C and under nitrogen pressures of 200–500 psi. The extrusion was carried out in stages using progressively smaller pore-size polycarbonate membranes (Whatman Inc, UK), with several cycles per pore-size, to achieve unilamellar vesicles in a final size range of ~100 nm in diameter. Lipid mass was quantified as previously reported¹⁷. MTX was assayed at 303nm using a UV spectrophotometer (Cary 5000).

2.2.3. Surface modification of NPs

The surface modification was carried out on the NPs, according to our previously reported procedures²². Briefly, HMw-HA (700

KDa) or LMw HA (8.9 kDa) (Lifecore Biomedical LLCChaska, MN, USA) was dissolved in 0.2 M MES buffer (pH 5.5) to a final concentration of 5 mg/ml. HA was activated with EDC and sulfo-NHS at a molar ratio of 1:1:6. After 30 min of activation the lipid NPs were added and the pH was adjusted to 7.4. The solution was incubated at room temp (2 h). The free HA was removed by 3 cycles of repeated washing by centrifugation (1.3×10^5 g, 4 °C, 60 min).

2.2.4 Entrapment of MTX in tsNPs and release profile.

The kinetics of drug efflux was studied as previously described¹⁵⁻¹⁸. Briefly, a suspension of tsNPs or NPs (0.5–1.0 ml) was placed in a dialysis sac and the sac was immersed in a continuously stirred receiver vessel, containing drug-free buffer (HBS at pH 7.4). The buffer volume in the receiver vessel was 10- to 16-fold higher than that of the tsNPs sample in the dialysis sac. At designated periods, the dialysis sac was transferred from one receiver vessel to another, containing fresh (i.e., drug free) buffer. Drug concentration was assayed in each dialysate and in the sac (at the beginning and end of each experiment). In order to obtain a quantitative evaluation of drug release, experimental data were analyzed according to a previously derived multi-pool kinetic model^{21, 23}, in which drug efflux from the sac into the reservoir occurs from a series of independent drug pools, one corresponding to free (i.e., unencapsulated) drug, and all others to tsNPs-associated drug. The overall drug release corresponds to the following equation:

$$f(t) = \sum_{j=1}^n f_j (1 - \exp^{-k_j t})$$

Where t denotes time, $f(t)$ is the cumulative drug released into the dialysate at time t , normalized to the total drug in the system at time 0, f_j is the fraction of the total drug in the system occupying the j 'th pool at time = 0, and k_j is the rate constant for drug diffusion from the j 'th pool.

The data analysis of efflux kinetics is also used to calculate the encapsulation efficiency. As discussed above, magnitudes of the parameter f_j are obtained through data analysis. When the efflux experiment is carried out on samples from the complete lipid NP preparation, the sum of $f_j(s)$ for the pool(s) of encapsulated drug is also the efficiency of encapsulation.

MTX conc. Was assayed by UV spectrophotometer (Cary 5000) at 303nm.

2.2.5. Particle size distribution and zeta potential measurements

Particle size distribution and zeta potential measurements were determined by light scattering using Malvern nano ZS Zetasizer (Malvern Instruments Ltd. Worcestershire, UK). Size measurements were performed in HBS pH 7.4 and zeta potential measurements were performed in 0.01XHBS pH 7.4. Each experimental result was an average of at least six independent measurements.

2.2.6. Cell culture growth and maintenance

Monolayers of B16F10 (murine skin melanoma) cells were grown in 100 × 20 mm dishes as previously reported^{17, 24}. The cells were cultured in Dulbecco's modified Eagle's medium (DMEM) containing 10% fetal bovine serum, Penicillin

(100 U/ml), Streptomycin (0.1 mg/ml), Nystatin (12.5 U/ml) and l-glutamine (2 mM). Cells were free of Mycoplasma contamination as determined by a Mycoplasma PCR test carried out every 3 months. Viability of cultures used in the experiments was > 90%, as determined by the trypan blue method.

2.2.7. Flow cytometry analysis of surface CD44

Flow cytometry of cell surface CD44 antigens was performed as previously described^{17, 18}. The following mAbs were used: Alexa Fluor 488-conjugated Rat anti-human CD44 (clone # IM7) and IgG2b isotype control. Data were acquired on FACScan with CellQuest software (Becton Dickinson, Franklin Lakes, NJ). Data analysis was performed using FlowJo software (Tree Star, Inc. Oregon, USA).

2.2.8 tsNPs binding to cell monolayers - confocal microscopy analysis

Analysis of tsNPs binding to B16F10 cells was performed in 24 well plates as previously described²². Briefly, 7.0×10^4 B16F10 cells were seeded on cover slips in growth media. The cells were exposed to Cy5 labeled NPs or tsNPs (25 µg) in medium without serum for a period of 1 h at 37 °C in a humidified atmosphere with 5% CO₂. Subsequently, the cells were washed twice using cold PBS, fixated with 4% PFA and washed again with cold PBS. ConA 488 (Life Technologies) staining was performed according to manufacturer instructions. The cells were mounted using the fluorescent mounting medium (Golden Bridge international, Mukilteo, WA, USA) and the fluorescence was assessed using a confocal microscope (LEICA TC SP5 II STED) with spatial resolution of 50-70 nm. Serial optical sections of the cells were recorded for each treatment and the images were processed using the Leica Application Suite LAS-AF Lite software (Leica Microsystems Inc.).

2.2.9 Animal Treatment

Animals were obtained from the animal breeding center, Tel Aviv University (Tel Aviv, Israel). Animals were maintained and treated according to National Institutes of Health guidelines. All animal protocols were approved by the Tel Aviv Institutional Animal Care and Use Committee.

2.2.10 Cytokine induction assay *in vivo*

NPs or tsNPs were injected intravenously to C57BL mice at a dose of 90mg/kg. Lipopolysaccharide (LPS, Sigma) at a concentration of 1mg/ml (100µl) was used as positive control. Two hours post injection whole blood was collected and animals were scarified. After collection, whole blood was allowed to clot by leaving it undisturbed at RT for 30 minutes. The clot was removed by centrifugation for 10 minutes at 1000Xg. The supernatant was transferred to a new tube and stored at -80°C prior to the cytokine analysis.

An hour before the analysis, the samples were thawed, diluted 1:2 in the diluents solution provided by the manufacturer and analyzed according to the manufacturer instructions, using a Milliplex® MAP kit 25-plex Mouse cytokine/chemokine Magnetic bead panel (MCTOMAG-70K-PMX, Millipore). The following cytokines were assessed: G-CSF, GM-CSF, IFN-γ, IL-10, IL-12 (p40), IL-12 (p70), IL-13, IL-15, IL-17, IL-1α, IL-1β, IL-2, IL-4, IL-5, IL-6, IL-7, IL-9, IP-10, KC, MCP-1, MIP-1α, MIP-1β, MIP-2, RANTES, TNF-α. Cytokines levels were read on

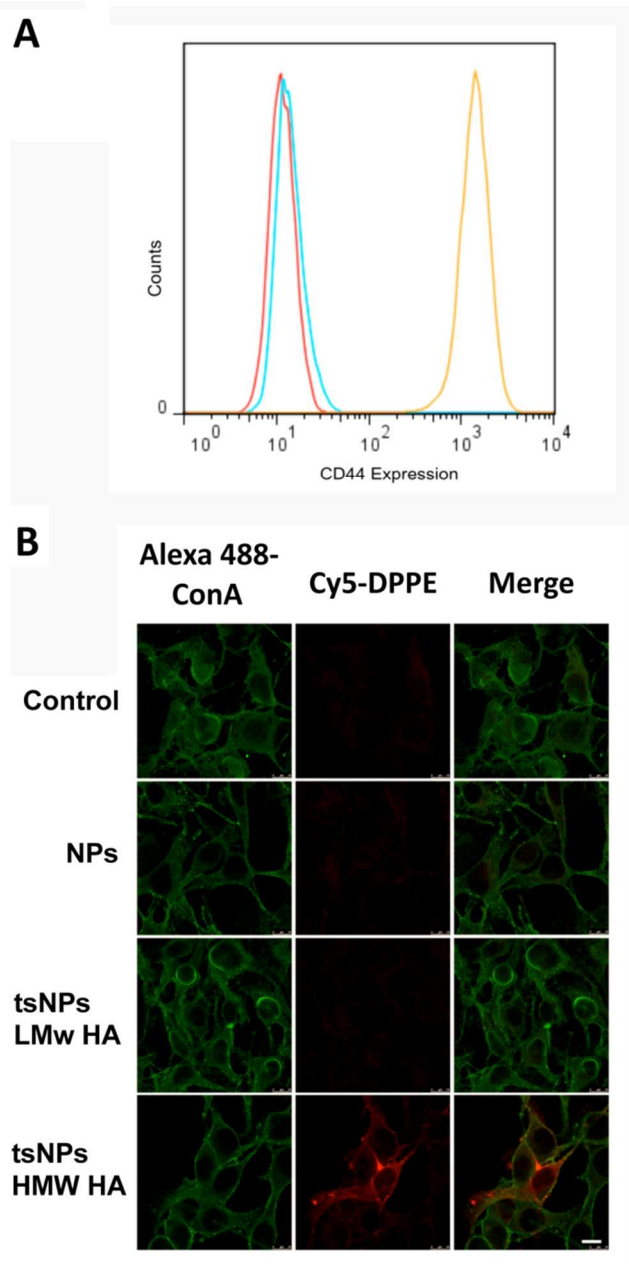


Figure 1: HMw HA-tsNPs selectively bind to B16F10 cells

A. Representative FACS histogram of CD44 expression in B16F10 cells is presented. Cells were stained with isotype control antibody (blue curve), or with Alexa Fluor 488 anti CD44 and IgG2b isotype control. Control, non-stained cells are presented by red curve. B. Representative confocal images of binding of Cy5 labeled NPs and tsNPs to B16F10 cells. Cells were seeded onto 6 well plates and incubated with 25 μ g of Cy5 labeled NPs- LMw HA tsNPs or HMw HA tsNPs for 1h at 37 $^{\circ}$ C. Cell membranes were labeled with Alexa 488 ConA. Bar 10 μ m.

the Luminex 200 System, Multiplex Bio-Assay Analyzer (Millipore, MA, USA). The quantification was done based on standard curves for each cytokine in the concentration range of 3.2-10,000 pg/mL.

2.2.11 Syngeneic SC tumor model

10-12 week old female C57BL/6 mice were maintained under specific pathogen-free (SPF) conditions. Tumors were induced by subcutaneous injection of 2×10^5 B16F10 cells in HBSS SC into the flank region of the mice. Tumors reached ~ 40 - 50 mm 3 10-12 days post injection. For biodistribution studies, Cy5 labeled NPs or tsNPs were injected intravenously (i.v.) to tumor bearing mice using a 27-gauge needle at a dose of 90mg/kg. 3.5, 24 and 48 hours post injection mice were sacrificed and the liver, lungs, spleen, heart and kidneys were isolated and scaled organ fluorescent signals per area were analyzed using the Maestro in vivo fluorescence imaging system (Perkin Elmer, Inc.). For histological hematoxylin and eosin (H&E) analysis tumors were fixed in 10% formalin in PBS over night at RT, embedded in paraffin and cut into 5 μ m sections.

For determination of NP and tsNPs tumor localization, tumors were isolated 3.5, 24 and 48 hours post NPs or tsNPs injection. The tumors were fixed in 10% buffered formalin in PBS ON at RT and transferred to 30% over night at 4 $^{\circ}$ C. The tumors were embedded in OCT and cut into 5 μ m sections. Images were obtained using the confocal microscope LEICA TC SP5 II STED with spatial resolution of 50-70 nm. Tumor fluorescence signals per area were analyzed using the Leica Application Suite LAS-AF Lite software.

2.2.12 Therapeutic efficacy studies

Treatments were initiated 12 days post tumor inoculation, when tumor volumes reached ~ 40 mm 3 (day 0). Tumor volume was calculated as: (width) 2 x length/2. The mice were randomly separated into four groups (n = 6/group): 1) HBS, 2) free MTX, 3) NPs entrapping MTX, 4) LMw HA-tsNPs entrapping MTX and 5) HMw HA-tsNPs entrapping MTX. The doses in the free MTX and in all the tsNPs formulations were 0.25mg/kg body and treatments were given every other day for 5 times. Administration was by i.v. injection of 100 μ l of the selected formulation to the lateral tail vein, using a 27-gauge needle. Tumors dimensions were assayed by electronic caliper as previously reported.

2.2.13 Statistical analysis

Results are expressed as mean \pm SD. Differences between two means were tested using an unpaired, two-sided Student's t-test. Differences between treatment groups were evaluated by one-way ANOVA with significance determined by Bonferroni adjusted t-test.

3. Results and discussion

3.1 Structural characterizations of NPs and tsNPs

In order to investigate the effect of surface anchored HA Mw on NP cellular targeting, biodistribution and immune modulation, we prepared three types of NPs: uncoated lipid NPs, lipid NPs coated with LMw HA (LMw HA-tsNPs) and lipid NPs coated with HMw-HA (HMw HA-tsNPs). The structural characteristics of all NPs are summarized in Table 1.

Surface modification of lipid NPs with HA did not lead to a significant change in NP size, however, a significant decrease in the zeta potential of the NPs was detected from -8mV to < -21mV. This decrease in the zeta potential is in line with the surface modification with the negatively charged HA.

Cite this: DOI: 10.1039/c0xx00000x

www.rsc.org/xxxxxx

PAPER

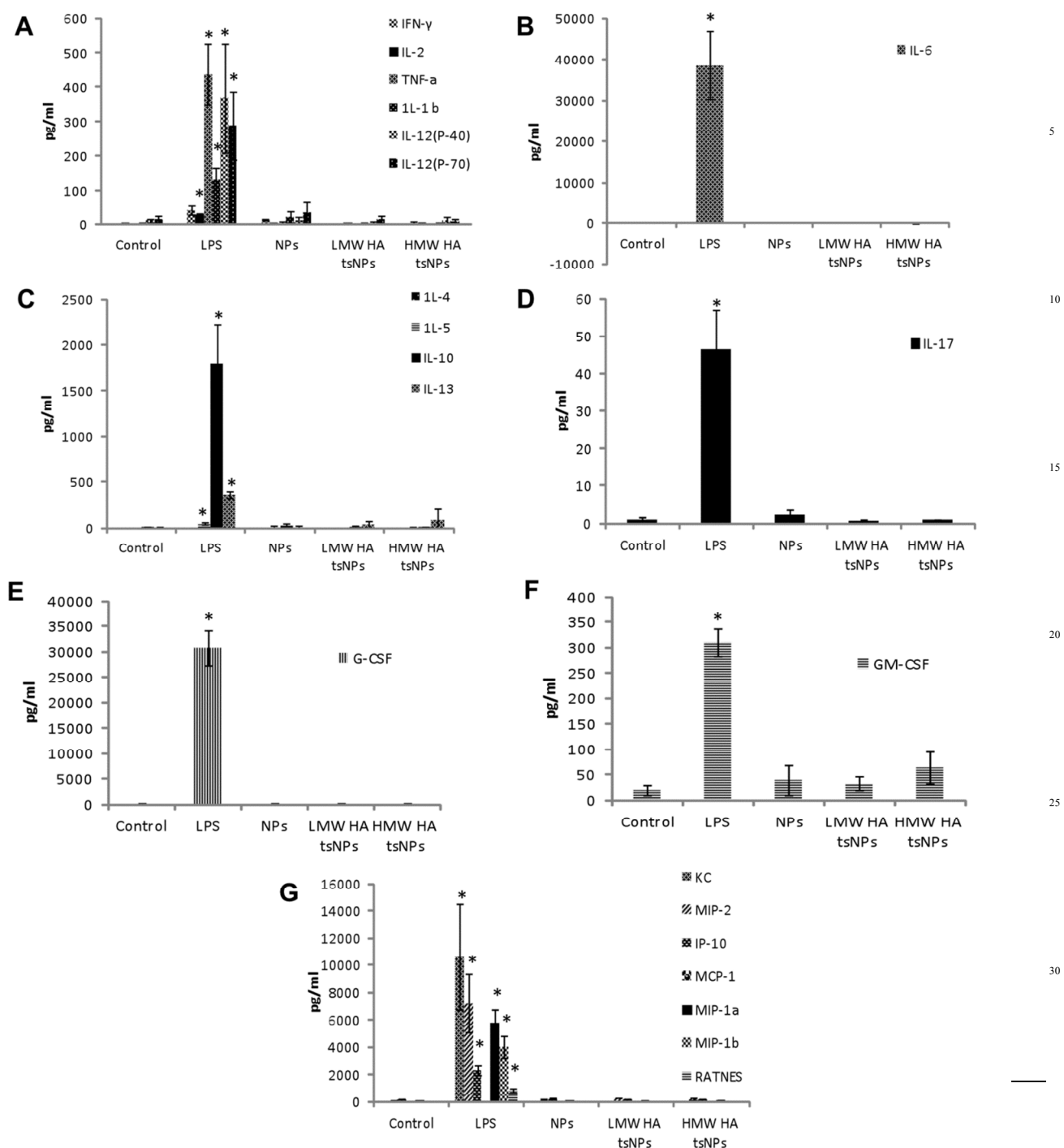


Figure 2: tsNPs do not trigger cytokine release when injected systemically NPs and tsNPs were injected i.v. to C57BL mice. Two hours post injection, serum was isolated and cytokine levels were measured using ELISA array. A-B. Pro-inflammatory cytokines and Th1 response. C. Th2 response D. Th17 response. E-G. Growth factors and chemokines. * denoted $p < 0.05$

Cite this: DOI: 10.1039/c0xx00000x

www.rsc.org/xxxxxx

PAPER**Table 1.** Physicochemical characteristics of NPs, tsNPs coated with LMw HA and tsNPs coated with HMw HA. The measurements were performed using Malvern Nano ZS zetasizer as described in the materials and methods section.

| Particle | Hydrodynamic Diameter (nm) | Zeta potential (mV) |
|--------------|----------------------------|---------------------|
| NPs | 166±20 | -8.4±2.5 |
| LMw HA-tsNPs | 169±25 | -21.2±3.5 |
| HMw HA-tsNPs | 190±35 | -22.7±3 |

Each results is an average ± SD of at least 6 independent measurements. Batch-to-batch variability was small, within the range reported for this particular batch.

3.2 HMw HA-tsNPs selectively bind to B16F10 cells *in vitro*

The covalent attachment of HA to the surface of the NPs did not impair the ability to bind to CD44 receptor, as we have shown previously⁷. As we have reported, coating NPs with HA provokes their binding to recombinant human CD44-Fc chimera immobilized to carboxymethylated dextran sensor chip (CM5) using SPR analysis⁷. We have demonstrated that the affinity of tsNPs towards the immobilized CD44 was solely controlled by the Mw of the surface anchored HA. While LMw-HA-tsNPs were characterized with extremely low binding, HMw-HA-tsNPs bind to the immobilized CD44 with high affinity. Here we present the effect of anchored HA Mw on binding to B16F10 cells (Figure 1). B16F10 cells were used due to the high expression of the HA receptor CD44, a feature of many cancer cells. The expression level of CD44 in B16F10 was demonstrated by flow cytometry as described in the experimental section (Figure 1A).

In order to test the NPs and tsNPs in an in-vitro setting, one of the lipids (DPPE) in the formulation (both in NPs and tsNPs) was labeled with Cy5 and incorporated into the preparation of the NPs (at 0.1% mol). The cells were incubated in the presence of tsNPs for 1h at 37 °C as described in the experimental section and the binding of tsNPs was analyzed by confocal microscopy. As seen in Figure 1B, surface bound HA retained its affinity towards the HA receptor CD44 and this affinity is directly related to the Mw of the surface HA. While the Cy5 labeling is hardly detectable for cells incubated with NPs or LMw-HA-tsNPs, incubation with HMw-HA-tsNPs resulted in significant fluorescence mostly at the cell membrane. This clearly indicates specific binding of the HMw-HA-tsNPs and correlates with our previously obtained SPR results⁷.

3.3 tsNPs do not trigger cytokines release when injected systemically

Unlike LMw-HA that has shown to induce inflammatory responses, HMw-HA is believed to play a homeostatic role²⁵. As was shown for fragments of other extracellular matrix (ECM) components⁴, upon tissue destruction, HMw-HA is broken down to fragments that can activate inflammatory responses. LMw-HA was shown to stimulate macrophages recruited to sites of inflammation and to produce important mediators of tissue injury and repair²⁶⁻²⁸. In addition to macrophages, several studies demonstrated induction of pro-inflammatory responses by LMw-HA of other cell types such as epithelial cells, endothelial cells, fibroblasts, and dendritic cells²⁵. The genes induced by LMw-HA include the cytokines (TNF- α , IL-6, IL-12 and IL-8), chemokines (MIP-1 α , MIP-1 β , KC, RANTES, MCP-1, and IFN-inducible protein-10), reactive nitrogen species and several growth factors^{25, 26, 29}.

Nevertheless, literature reports regarding general pro-inflammatory effects by HA and specific effects on macrophage activation are not consistent. HMw-HA was shown to induce TNF- α production by RAW 264.7 cell line and by primary (peritoneal) macrophages³⁰ while in another study that was performed also on RAW 264.7 cell line there were no induction of pro-inflammatory cytokines regardless of the HA Mw tested¹⁰. Therefore, we have previously tested whether tsNPs with different surface anchored HA Mws can induce macrophage activation⁷. We monitored the levels of secreted TNF- α and IL-10 from RAW 264.7 macrophages following incubation with NPs or tsNPs. We chose to monitor the levels of TNF- α since it is the first cytokine to be released after activation of essentially all Toll – Like Receptors (TLRs) and is regarded as the key pro-inflammatory cytokine^{20, 31}. In addition, TNF- α also enhances the production of the key anti-inflammatory cytokine IL-10³², which in turn suppresses TNF- α to complete the negative regulatory feedback cycle. No cytokine induction was observed regardless of the HA Mw anchored to the NPs' surface⁷.

In this study, we tested the effect of NPs and tsNPs on induction of cytokines *in vivo* upon a single intravenous (i.v.) administration. For this task, NPs and tsNPs were injected i.v. to C57BL mice. LPS, a potent TLR4 activator that mediates acute inflammation^{27, 33, 34}, was used as positive control since as with short fragments of HA, the initiated inflammatory responses is facilitated by TLR4³³. Serum cytokine levels were measured using a Milliplex® MAP kit 25-plex Mouse cytokine/chemokine Magnetic bead panel as described in the experimental section (Figure 2). In order to achieve a better understanding of the influence of the NPs and tsNPs on the immune response, the cytokines panel measured was largely extended in comparison to our previous study and included the following cytokines, chemokines and growth factors: TNF- α , INF- γ , IL-2, IL-1 β , IL-12 (p40), IL-12 (p70), IL-6, IL-4, IL-7, IL-5, IL-9, IL-10, IL-15, IL-13, IL-17, KC, MIP2-a, IP-10, MCP-1, MIP-1 α , MIP-1 β ,

Cite this: DOI: 10.1039/c0xx00000x

www.rsc.org/xxxxxx

PAPER

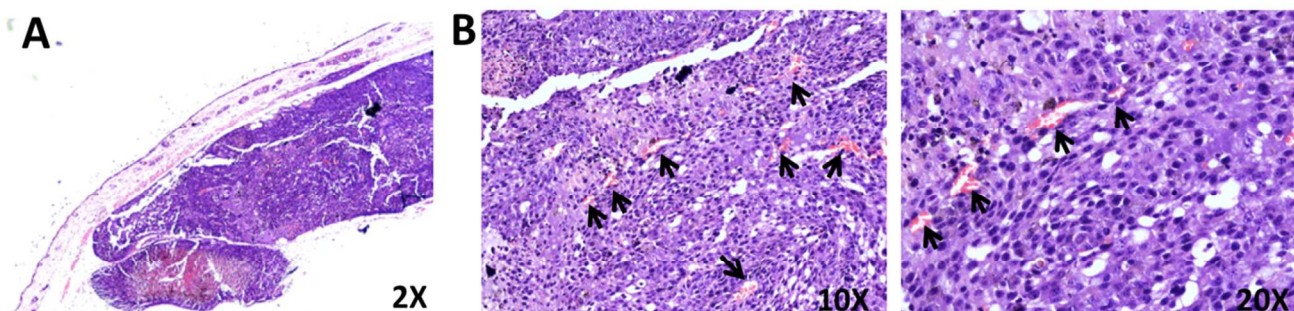


Figure 3: H&E staining of SC B16F10 tumors. A. Representative image of B16F10 SC tumor. B. Tumor vasculature. Arrows indicate newly formed blood vessels. 2×10^5 B16F10 cells were injected subcutaneously to C57BL mice. The tumors were removed 7d post cell injection, fixed in formaldehyde and embedded in parathion. Sections were stained with H&E.

RANTES, G-CSF and GM-CSF (Figure 2). No induction of cytokines was observed regardless of the surface HA Mw of the tsNPs. These results contradict previous studies, which related LMw HA with macrophage activation and induction of cytokines. However, the result can be explained by the fact that the HA tested was covalently attached to the surface of the lipid NPs by a stable amide bond. Bound HA may be less potent in comparison to free HA as it can hurdle processing by cells and as a result impair macrophage activation. The discrepancy regarding the influence of LMw HA on the immune response should also be addressed. Stern et al.⁵ discussed this issue and detailed several intrinsic challenges to the study of HA fragments. These challenges include inaccurate measurements of HA fragment Mw, HA sample preparation as it may affect HA conformation and non HA contamination for HA of animal or bacterial origin⁵. In addition, all evidence of the biological effects of HA fragments were based on exogenous addition of HA fragments and no evidence exist regarding the ability of cells to release, synthesize or even internalize LMw HA⁵.

3.4 HMw-HA- tsNPs accumulate in B16F10 tumor bearing mice

3.4.1 Establishment of a syngeneic subcutaneous tumor model

In order to test differences in biodistribution of NPs and tsNPs in solid tumors we have established a syngeneic subcutaneous (SC) B16F10 tumor model in C57BL mice. Syngeneic tumor model offer several advantages over human exnograf models. They are reproducible, they enable to use immunocompetent hosts and therefore better represent natural tumor surrounding and they are generally nonimmunogenic³⁵. The main disadvantages of syngeneic tumor models are that the tumor cells are rodent, and therefore express the mouse/rat homologues of the desired targets³⁵. However, in our case this disadvantage is not relevant as the ligand for both murine and human CD44 is Hyaluronan. For this purpose, the highly expressing CD44 cells B16F10 (Figure 1A) were injected SC and tumors were formed a 10-12 days post injection. The obtained tumors contained multiple newly formed

blood vessels (Figure 3), thus this is an ideal model to test the EPR effect of small NPs and the contribution of HA as the coating ligand to target the tumor via passive (EPR) and active cellular targeting mechanisms. Pathology examination revealed SC tumors in the mice injected with B16F10 cells whereas their lungs, spleens, kidneys, and livers were found to be tumor-free.

3.4.2 tsNPs are detected in organs after 48 h post administration in B16F10 tumor bearing mice

Literature reports that discuss the influence of free HA Mw on biodistribution performed in healthy mice/rats^{36, 37} revealed longer circulation time for the HMw HA. In addition, there were differences in the biodistribution- higher amounts HMw HA-111In-DTPA conjugates were taken up by the liver in comparison to the LMw HA-111In-DTPA conjugates that were found in the urine probably due to non enzymatic cleavage³⁷. Upon conjugation to the surface of NPs, HMw have been shown to significantly increase the NP's circulation time as it provides a protective hydrophilic coating, similar to the frequently used polyethylene glycol (PEG) and inhibits reticuloendothelial system (RES) uptake^{15, 16}. In order to test the differences in biodistribution profile between NPs and tsNPs in tumor bearing mice, Cy5 labeled NPs and tsNPs were injected i.v. and the fluorescence intensity of isolated organs was measured 3.5 and 24 hours post injection by the Maestro in vivo fluorescence imaging system (Figure 4). The NPs and tsNPs were labeled by incorporation of Cy5 conjugated-DPPE that was incorporated into the lipid mixture of the NPs as detailed in the experimental section. No significant difference in the signals of isolated RES organs (Liver, spleen, and lungs) from tumor bearing mice was observed between NPs, HMw-HA tsNPs and LMw-HA tsNPs at the measured time points (Supplementary Figure 1 and Figure 4).

3.5 HMw-HA- tsNPs specifically target B16F10 tumor bearing mice.

In order to test the effect of NPs and tsNPs on tumor localization, Cy5 labeled NPs and tsNPs were injected i.v. into B16F10 tumor

Cite this: DOI: 10.1039/c0xx00000x

www.rsc.org/xxxxxx

PAPER

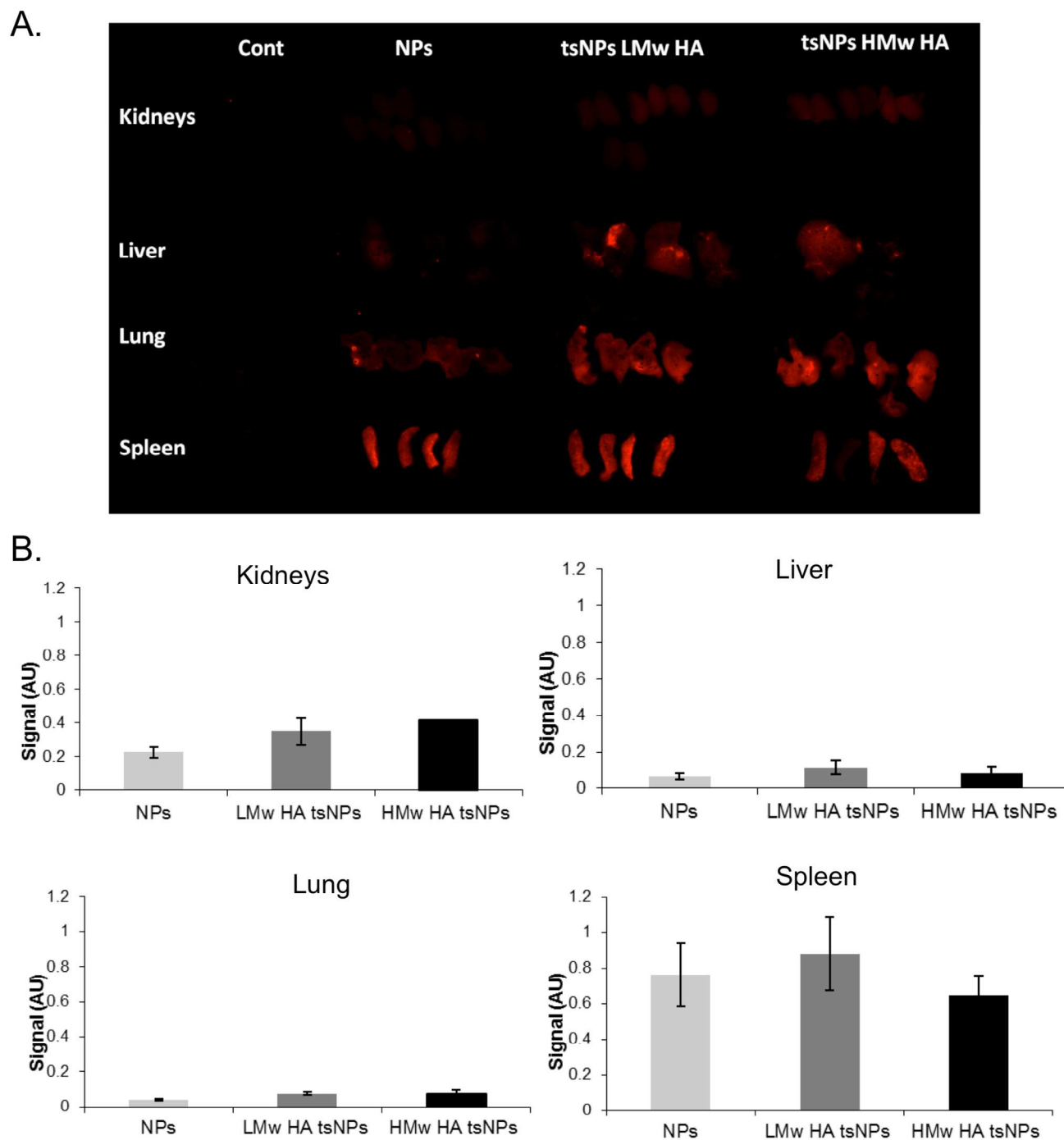


Figure 4: Biodistribution of NPs and tsNPs in B16F10 SC tumor bearing mice. Mice were injected with PBS, Cy5 labeled NPs or tsNPs. 24 hours post injection mice organs were isolated and fluorescent signals were measured as described in the experimental section. A. Isolated organs B. The scaled fluorescent signal levels per area of isolated organs were measured by Maestro in vivo fluorescence imaging system

Cite this: DOI: 10.1039/c0xx00000x

www.rsc.org/xxxxxx

PAPER

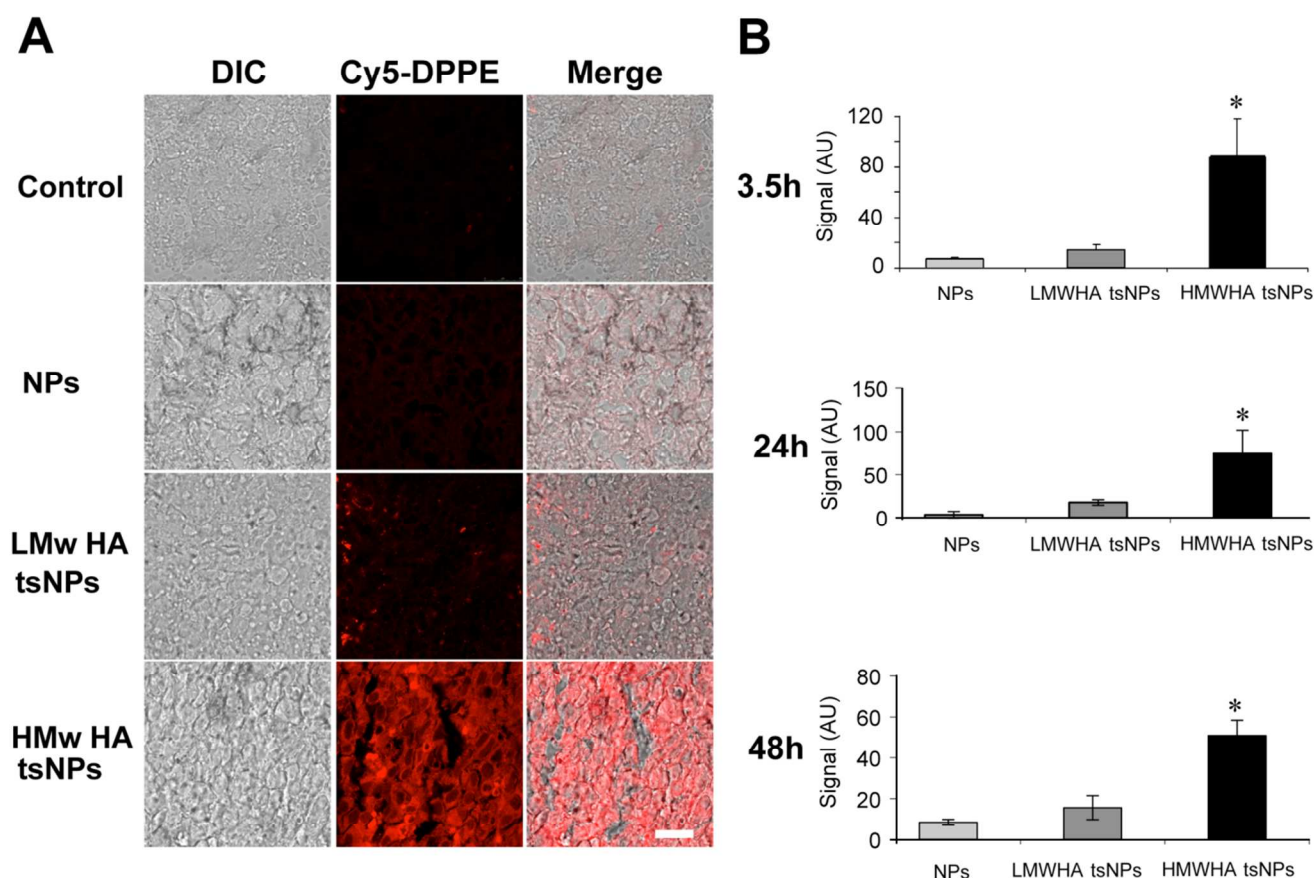


Figure 5: Tumor localization of NPs and tsNPs post intravenous injection. A representative confocal images of B16F10 isolated tumors 24h post i.v. injection of Cy5 labeled NP and tsNPs. Bar scale 25 μ m. B16F10 tumor bearing mice were i.v. injected with Cy5 labeled NPs and tsNPs. 24 hours post injection tumors were isolated, fixed in formalin and embedded in OCT. Sections were analyzed by confocal microscopy as described in the experimental section. B. Representative tumor fluorescent signals per area obtained from confocal analysis 3.5, 24 and 48 hours post i.v. injection of Cy5 labeled NPs and tsNPs to B16F10 tumor bearing mice.

bearing mice. Tumors were isolated and the signals were analyzed by confocal microscopy as detailed in the methods section (Figure 5). The highest tumor signals were obtained with 10 HMw HA coated tsNPs in all time points tested (3.5h, 24h and 48h) (Figure 5). This can be attributed to a combination of passive targeting via the enhanced permeability and retention (EPR) effect that characterizes solid tumor and active targeting towards the HA receptor CD44 highly expressed on B16F10 cells 15 (Figure 1). The effect of NP surface anchored HMw-HA on promoting long circulation of NPs has been shown¹⁵ and is related to the hydroxyl residues of HA that endow the NPs with a hydrophilic coat that reduces the attachment of circulating serum opsonins and subsequent clearance by the reticuloendothelial 20 system (RES).

The difference between LMw HA tsNPs and HMw HA tsNPs can be explained by the significantly lower binding to CD44 as

shown also in Figure 1 and our previously reported Surface plasmon resonance (SPR) data⁷. This can highlight the 25 importance of active tumor targeting via the CD44 receptor for promoting long circulation beyond the passive targeting obtained by the EPR effect alone.

The LMw HA coating on the NPs increases tumor localization signal, however the difference between NPs and LMw HA coated 30 NPs is not significant.

3.6 HMw HA-tsNPs entrapping MTX enhance the therapeutic response in a B16F10 melanoma bearing mice.

After confirming that there is no statistical difference between 35 tumor accumulation of NPs and LMw HA-tsNPs 48 h post i.v. administration and substantial accumulation of the HMw HA-tsNPs in the tumor, we hypothesize that entrapping a therapeutic payload within the HMw HA-tsNPs should show an improved

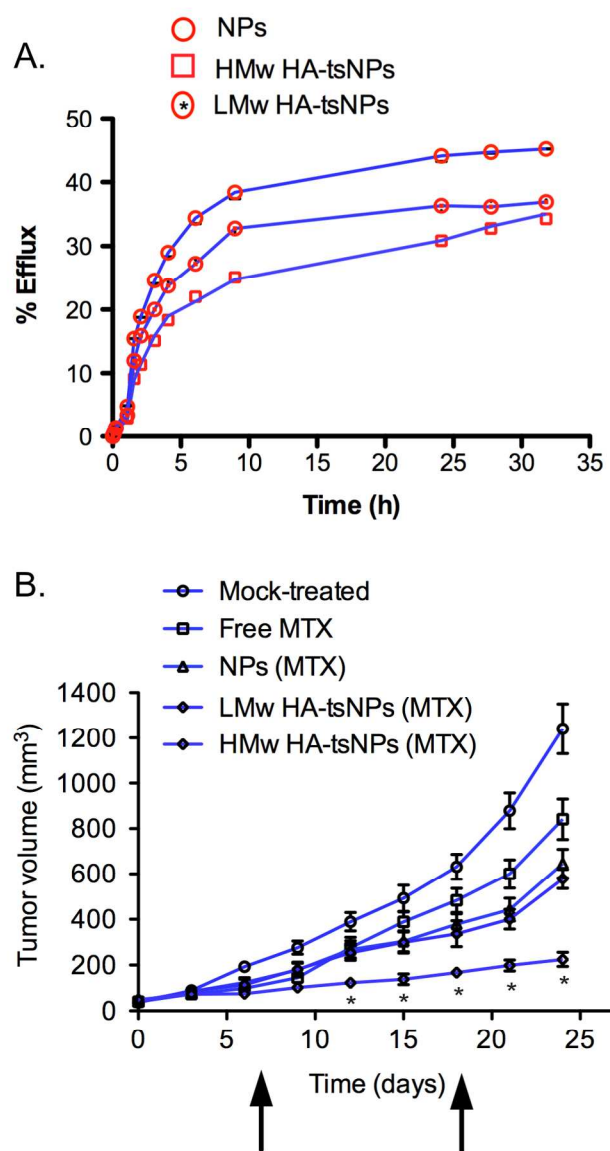


Figure 6. Enhanced therapeutic response with HMw HA-tsNPs entrapping MTX in B16F10 melanoma model.

A. MTX release profile from HMw HA-tsNPs and NPs. The points are experimental, each an average of duplicates and the solid curves are the theoretical expectations, the results are of data analysis according to equation (1) (as described in the experimental section) for the case of $n=2$. B. Therapeutic efficacy was demonstrated using i.v. injections every other day for 5 times post initiation of the experiment with doses and formulations as listed in the experimental section. Data are expressed as the mean \pm SEM of ($n = 6/\text{group}$). * $p < 0.001$. Arrows represent starting and ending treatment.

therapeutic response which is beyond the effect of the EPR. The hydrophilic chemotherapy MTX was chosen as a surrogate marker to test this hypothesis. We tested in vivo the following groups: Mock-treated, free MTX, NPs entrapping MTX, LMw HA-tsNPs entrapping MTX and HMw HA-tsNPs entrapping

MTX.

We first entrapped MTX in the particles and characterized their size distribution and zeta potential (Table 2).

Encapsulation of MTX did not change significantly the size distribution of the particles (Table 2) nor its zeta potential indicating that the drug is entrapped in the aqueous phase of the particles. The zeta potential measured to LMw HA-tsNPs and HMw HA-tsNPs was similar (Table 2). This is an expected observation since the amount of carboxyl group is similar for HMWHA and LMWHA since we used equal weights and was already observed for the particles without the entrapped drug (Table 1).

Table 2. Physicochemical characteristics of NPs and tsNPs coated with LMw HA or HMw HA entrapping MTX. The measurements were performed using Malvern Nano ZS zetasizer as described in the materials and methods section.

| Particle | Hydrodynamic Diameter (nm) | Zeta potential (mV) |
|---------------------|----------------------------|---------------------|
| NPs (MTX) | 159 \pm 28 | -7.8 \pm 1.5 |
| LMw HA-tsNPs | 167 \pm 11 | -22.1 \pm 3.1 |
| HMw HA- tsNPs (MTX) | 189 \pm 39 | -24.1 \pm 4.4 |

Each results is an average \pm SD of at least 6 independent measurements. Batch-to-batch variability was small, within the range reported for this particular batch.

Next, we monitored the drug release profile in vitro as detailed in the experimental section.

MTX release profile from the NPs, LMw HA-tsNPs and HMw HA-tsNPs (Figure 6A) was processed according to equation (1) and found to fit the case of 2 drug pools (i.e., $n=2$) with a rather fast dissipation of unencapsulated MTX and significantly slower efflux of the encapsulated MTX. The rate constant determined for the efflux of encapsulated MTX from NPs, LMw HA-tsNPs and HMw HA-tsNPs were $2.8 \times 10^{-3} \text{ hours}^{-1}$, $2.6 \times 10^{-3} \text{ hours}^{-1}$ and $2.2 \times 10^{-3} \text{ hours}^{-1}$ corresponded to half-life of 10, 11 and 13.75 days, respectively. It is likely that the high molecular weight HA is serving as an additional reservoir of MTX since the diffusion of MTX from these particles is substantially slower than from LMw HA-tsNPs or the non-coated NPs. The MTX encapsulation efficiency was 60(\pm 4) %, 63(\pm 2)% and 69.4 (\pm 5.5) % for NPs, LMw HA-tsNPs and HMw HA-tsNPs, respectively.

Next, we studied the therapeutic effect of HMw HA-tsNPs entrapping MTX in comparison to the free MTX and of MTX entrapped in NPs in B16F10 bearing mice. Tumors were obtained \sim 12 days post tumor inoculation, and mice ($n = 6/\text{group}$) were i.v. administrated with: 1) HBS, 2) free MTX, 3) NPs entrapping MTX, 4) LMw HA-tsNPs entrapping MTX and 5) HMw HA-tsNPs entrapping MTX. The doses in the free MTX, NPs and the HMw HA-tsNPs formulations were 0.25mg/kg body, and treatments were given every other day for 10 consecutive days starting 7 days post mice randomization. Tumors volumes were monitored every 3 days using an electronic caliper. The MTX entrapped in HMw HA-tsNPs significantly ($p < 0.001$) attenuated

the growth of the tumors relative to the free MTX and MTX entrapped in NPs (Figure 6B) suggesting that EPR is not the dominant mechanism while treating with HMw HA-tsNPs but a combination of EPR (passive tumor targeting) via the newly formed blood vessels surrounding the tumor (See Figure 3) with active cellular targeting mechanism.

4. Conclusions

We have presented two types of lipid NPs distinguished only by the Mw of their surface anchored HA. LMw HA-tsNPs (<10kDa) and HMw HA-tsNPs (700kDa). The Mw of the surface anchored HA had a significant influence on the affinity towards the HA receptor CD44 on B16F10 murine melanoma cells *in vitro*. LMw HA-tsNPs exhibited a weak binding comparable to uncoated NPs while binding of HMw HA -tsNPs was characterized with high affinity. Both types of tsNPs, regardless of their surface anchored HA Mw, had no effect on triggering immune response as evident by low to minimal cytokine induction *in vivo* following intravenous administration to C57BL mice.

A significant effect of the tsNPs surface anchored HA Mw was also detected for tumor targeting and circulation time as the presence and duration of HMw HA-tsNPs greatly exceeded that of LMw HA-tsNPs and uncoated NPs. Finally, we demonstrated via an entrapment of MTX, a commonly used chemotherapy that the therapeutic effect in tumor bearing mice treated with HMw HA-tsNPs (trapping MTX) is substantially higher than any tested control. This highlights the importance of active tumor targeting via the HA receptor for promoting long circulation beyond the passive targeting obtained by the EPR effect alone. Taking together, these data suggest that HMw HA may have important implications for the development of future drug delivery systems using an active cellular targeting approach.

Acknowledgements

S.M. thanks TAU Nano Center for Ph.D. fellowship. This work was supported in part by the grants from the Lewis Family Trust, the Israeli Centre of Research Excellence (I-CORE), Gene Regulation in Complex Human Disease, Center No 41/11; Israel Science Foundation (Award 181/10); FTA: Nanomedicine for Personalized Theranostics, and by The Leona M. and Harry B. Helmsley Nanotechnology Research Fund awarded to D.P.

Notes and references

¹Laboratory of NanoMedicine, Department of Cell Research and Immunology, George S. Wise Faculty of Life Science, Tel Aviv University;

²Department of Materials Science and Engineering, Faculty of Engineering, Tel Aviv

University;

³Center for Nanoscience and Nanotechnology, Tel Aviv University, Tel Aviv 69978, Israel.

⁴School of chemistry, Tel Aviv University, Tel Aviv 69978, Israel.

⁵Houston Methodist Research Institute, Houston, TX, 77030, USA.

* Corresponding author: D.P. peer@tauex.tau.ac.il

† Electronic Supplementary Information (ESI) available: [details of any supplementary information available should be included here]. See DOI: 10.1039/b000000x/

1. A. Varki, *Essentials of glycobiology*, Cold Spring Harbor Laboratory Press, Cold Spring Harbor, N.Y., 2009.
2. B. P. Toole, *Nat Rev Cancer*, 2004, **4**, 528-539.
3. V. M. Platt and F. C. Szoka, Jr., *Mol Pharm*, 2008, **5**, 474-486.
4. T. L. Adair-Kirk and R. M. Senior, *Int J Biochem Cell Biol*, 2008, **40**, 1101-1110.
5. R. Stern, A. A. Asari and K. N. Sugahara, *Eur J Cell Biol*, 2006, **85**, 699-715.
6. P. M. Wolny, S. Banerji, C. Gounou, A. R. Brisson, A. J. Day, D. G. Jackson and R. P. Richter, *J Biol Chem*, 2010, **285**, 30170-30180.
7. S. Mizrahy, S. R. Raz, M. Hasgaard, H. Liu, N. Soffer-Tsur, K. Cohen, R. Dvash, D. Landsman-Milo, M. G. Bremer, S. M. Moghimi and D. Peer, *J Control Release*, 2011, **156**, 231-238.
8. H. Shigeishi, S. Fujimoto, M. Hiraoka, S. Ono, M. Taki, K. Ohta, K. Higashikawa and N. Kamata, *Int J Oncol*, 2009, **34**, 1565-1571.
9. S. Ogino, N. Nishida, R. Umamoto, M. Suzuki, M. Takeda, H. Terasawa, J. Kitayama, M. Matsumoto, H. Hayasaka, M. Miyasaka and I. Shimada, *Structure*, 2010, **18**, 649-656.
10. D. Krejcová, M. Pekarova, B. Safrankova and L. Kubala, *Neuro Endocrinol Lett*, 2009, **30 Suppl 1**, 106-111.
11. S. Mizrahy and D. Peer, *Chem Soc Rev*, 2012, **41**, 2623-2640.
12. G. Ouskova, B. Spellerberg and P. Prehm, *Glycobiology*, 2004, **14**, 931-938.
13. R. E. Eliaz and F. C. Szoka, Jr., *Cancer Res*, 2001, **61**, 2592-2601.
14. R. E. Eliaz, S. Nir and F. C. Szoka, Jr., *Methods Enzymol*, 2004, **387**, 16-33.
15. D. Peer and R. Margalit, *Neoplasia*, 2004, **6**, 343-353.
16. D. Peer and R. Margalit, *Int J Cancer*, 2004, **108**, 780-789.
17. D. Peer, E. J. Park, Y. Morishita, C. V. Carman and M. Shimaoka, *Science*, 2008, **319**, 627-630.
18. I. Rivkin, K. Cohen, J. Koffler, D. Melikhov, D. Peer and R. Margalit, *Biomaterials*, 2010, **31**, 7106-7114.
19. M. E. Jung and W. J. Kim, *Bioorg Med Chem*, 2006, **14**, 92-97.
20. R. Kedmi, N. Ben-Arie and D. Peer, *Biomaterials*, 2010, **31**, 6867-6875.
21. D. Peer and R. Margalit, *Arch Biochem Biophys*, 2000, **383**, 185-190.
22. D. Landesman-Milo, M. Goldsmith, S. Leviatan Ben-Arye, B. Witenberg, E. Brown, S. Leibovitch, S. Azriel, S. Tabak, V. Morad and D. Peer, *Cancer Lett*, 2013, **334**, 221-227.
23. R. Margalit, M. Okon, N. Yerushalmi and E. Avidor, *J Control Release*, 1992, **19**, 275-288.
24. D. Peer, Y. Dekel, D. Melikhov and R. Margalit, *Cancer Res*, 2004, **64**, 7562-7569.
25. K. A. Scheibner, M. A. Lutz, S. Boodoo, M. J. Fenton, J. D. Powell and M. R. Horton, *J Immunol*, 2006, **177**, 1272-1281.
26. M. R. Horton, M. D. Burdick, R. M. Strieter, C. Bao and P. W. Noble, *J Immunol*, 1998, **160**, 3023-3030.
27. C. M. McKee, M. B. Penno, M. Cowman, M. D. Burdick, R. M. Strieter, C. Bao and P. W. Noble, *J Clin Invest*, 1996, **98**, 2403-2413.

-
28. M. R. Horton, C. M. McKee, C. Bao, F. Liao, J. M. Farber, J. Hodge-DuFour, E. Pure, B. L. Oliver, T. M. Wright and P. W. Noble, *J Biol Chem*, 1998, **273**, 35088-35094.
29. H. Yamawaki, S. Hirohata, T. Miyoshi, K. Takahashi, H. Ogawa, R. Shinohata, K. Demircan, S. Kusachi, K. Yamamoto and Y. 5
Ninomiya, *Glycobiology*, 2009, **19**, 83-92.
30. M. J. Wang, J. S. Kuo, W. W. Lee, H. Y. Huang, W. F. Chen and S. Z. Lin, *J Neurochem*, 2006, **97**, 857-871.
31. B. Beutler, *Nature*, 2004, **430**, 257-263.
32. D. F. Fiorentino, A. Zlotnik, T. R. Mosmann, M. Howard and A. 10
O'Garra, *J Immunol*, 1991, **147**, 3815-3822.
33. D. Jiang, J. Liang, J. Fan, S. Yu, S. Chen, Y. Luo, G. D. Prestwich,
M. M. Mascarenhas, H. G. Garg, D. A. Quinn, R. J. Homer, D.
R. Goldstein, R. Bucala, P. J. Lee, R. Medzhitov and P. W. Noble, *Nat Med*, 2005, **11**, 1173-1179. 15
34. C. R. Amura, T. Kamei, N. Ito, M. J. Soares and D. C. Morrison, *J Immunol*, 1998, **161**, 2552-2560.
35. B. A. Teicher, *Mol Cancer Ther*, 2006, **5**, 2435-2443.
36. M. N. Courel, C. Maingonnat, P. Bertrand, C. Chauzy, F. Smadja-Joffe and B. Delpuch, *In Vivo*, 2004, **18**, 181-187. 20
37. E. Svanovsky, V. Velebny, A. Laznickova and M. Laznicek, *Eur J Drug Metab Pharmacokinet*, 2008, **33**, 149-157. 25

Cite this: DOI: 10.1039/c0xx00000x

www.rsc.org/xxxxxx

PAPER

Nanoscale Accepted Manuscript